IEEE Access
Multidisciplinary | Rapid Review | Open Access Journal

Received March 13, 2019, accepted April 9, 2019, date of publication May 7, 2019, date of current version June 4, 2019.

Digital Object Identifier 10.1109/ACCESS.2019.2915102

Velocity Optimization for Braking Energy Management of In-Wheel Motor Electric Vehicles

WEI XU[1,2], HONG CHEN[1,2], (Senior Member, IEEE), JUNMIN WANG[3], (Senior Member, IEEE), AND HAIYAN ZHAO[1,2]

[1]State Key Laboratory of Automotive Simulation and Control, Jilin University, Changchun, China
[2]Department of Control Science and Engineering, Jilin University, Campus Nanling, Changchun 130025, China
[3]Department of Mechanical Engineering, The University of Texas at Austin, Austin, TX 78712, USA

Corresponding author: Hong Chen (chenh@jlu.edu.cn)

This work was supported in part by the National Natural Science Foundation of China under Grant 61790564, Grant U1664257, and Grant U1564207, and in part by the Joint Project of Jilin Province and Jilin University under Grant SXGJSF2017-2-1-1.

ABSTRACT This paper presents two braking regenerative energy optimization controllers for in-wheel motor electric vehicles. The first one is a velocity-tracking controller based on a model predictive control (MPC) method to recover the braking energy. It takes the front and rears in-wheel motor efficiencies into account to distribute the hydraulic and in-wheel motor braking torque of the front and rear wheels. As the vehicle information and intelligence have brought new opportunities for energy management, another velocity optimization controller is designed by considering the restricted condition of terminal distance and terminal velocity. In this strategy, a receding-horizon MPC method is proposed to solve the restricted nonlinear optimal problem. Furthermore, this optimization algorithm is transformed from the time horizon to the distance horizon to satisfy the terminal distance constraint. AMESim/Simulink co-simulations are carried out to evaluate the effectiveness of the proposed controllers. The simulation results indicate that the velocity optimization method can achieve the braking requirement as well as effectively promote regenerative efficiency.

INDEX TERMS Electric vehicle, regenerative braking, energy management, model predict control.

I. INTRODUCTION

The global environment and energy issues have attracted increasing attention. As one of the new energy vehicle technologies, electric vehicles with the advantages of low carbonization, emissions have received a widespread attention from governments and companies [1], [2]. However, the limited driving range is a main reason hindering the applications of electric vehicles. In recent years, research about energy management system control of the electric vehicles has a major focus on energy efficiency and extending the driving ranges [3]–[5].

The regenerative braking control is one of the most important parts for an electric vehicle to extend its driving range by transferring the kinetic energy to electric energy. Currently, many studies on regenerative braking systems have been done. Ko *et al.* [6] presented a cooperative control strategy of three brake types, electronic wedge brake, electronic mechanical brake, and regenerative brake, for roads with different friction coefficients and deceleration conditions. Chen *et al.* [5] proposed a feedback hierarchical controller to improve the energy recovery. The upper-layer controller is to track the desired velocity of the vehicle, and the lower-layer controller is to allocate the braking torque between the front and rear wheels. In [7], three different regenerative braking control strategies are proposed and compared respecting to both braking comfort and regeneration efficiency. Simulations are carried out in a normal braking process and under the ECE (Economic Commission for Europe) driving cycle.

However, most researches of the regenerative braking control are about the cooperation of different braking modes, considering fixed decelerations or a driving cycle which are generally not applicable to actual situations. Moreover, the influence of varied velocity, road and traffic information to energy recovery are not considered in these research. Actually, the regeneration efficiency is related to many factors,

The associate editor coordinating the review of this manuscript and approving it for publication was Bin Zhou.

2169-3536 © 2019 IEEE. Translations and content mining are permitted for academic research only.
Personal use is also permitted, but republication/redistribution requires IEEE permission.
See http://www.ieee.org/publications_standards/publications/rights/index.html for more information.

such as the vehicle attributes, the road curve and slope and the driver behavior [8]. Kamal *et al.* [9] presented an model predictive control algorithm to obtain the the control inputs for an ecological vehicle on up-down slopes hilly road with no heavy traffic. Nowadays, the electric control technology of vehicles has become more intelligent based on the vehicle's onboard navigation system combining with global positioning system (GPS) and geographical information system (GIS) [10], [11]. Chen *et al.* [12] presented an energy management driving strategy based on the dynamic programming method with a terrain-information preview. The energy consumption for a given driving range is reduced by optimizing the motor torques and the velocity with no terminal velocity constraint. In [13], a bi-level MPC method is proposed to improve the energy management of a hybrid electric vehicle. The outer-loop optimizes the velocity considering the traffic information. The optimal torque split ratio is obtained in the inner-loop according to the optimal velocity. The cost function of the braking force which committed to reduce the braking process in the outer loop limits the possibility of energy recovery.

In this paper, a regenerative braking algorithm is designed to improve the energy recovery of a braking process for four in-wheel motors electric vehicles. First, a MPC based velocity-tracking controller is presented. Furthermore, considering the effect of mutative velocity of the braking process on the energy recovery, a velocity optimization controller is proposed based on the receding- horizon MPC method. The road slope and traffic information are supposed to be obtained by GPS and GIS, which are considered as the terminal braking distance and velocity in this strategy. This optimization problem is formulated by maximizing the regenerative energy with the constraints of the terminal braking distance and velocity and the control variable of the actuator. Based on the MPC method, the real-time solutions of braking torque and velocity trajectory are obtained for the optimization problem. It is not easy to solve this problem with the terminal distance constraint in normal time horizon. This is because that we consider the velocity as a variable in this problem. The terminal time will be a potential optimization variable but not a specific value. Therefore, the optimization problem is transferred from the time horizon to the distance horizon to satisfy the terminal distance constraint. The motor-to-battery efficiency difference between the front and rear wheels is considered in the cost function to optimize the energy recovery. In addition, the terminal velocity constraint is set as a terminal state penalty term while a receding-horizon MPC method is employed to solve this optimization problem. A strategy of receding-horizon with different sampling steps according to the varied velocity is used to reduce the prediction state errors caused by the sampling distance step.

The rest of this paper is organized as follows. In the second section, the model of an electric vehicle with four in-wheel motors equipped with a regenerative braking system is introduced. The regenerative energy optimization problem is formulated based on the system dynamics model. In the third section, the MPC based velocity-tracking controller and the velocity optimization controller are presented. In the forth section, the proposed regenerative braking control strategies are evaluated through the co-simulations based on AMESim and Simulink/Matlab platform. Finally, the conclusions are presented in the fifth section.

II. OPTIMIZATION PROBLEM STATEMENT AND CONTROL-ORIENTED MODELING

A. REGENERATIVE BRAKING SYSTEM OF ELECTRIC VEHICLES

The regenerative braking system structure of a four in-wheel motors electric vehicle is given in Fig. 1. It includes a vehicle control unit, a motor and battery unit and a hydraulic unit.

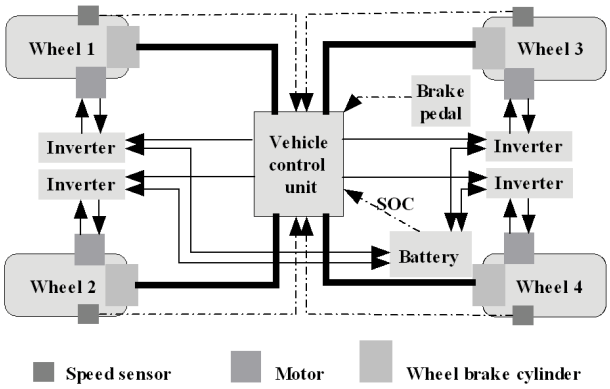

FIGURE 1. Hybrid braking structure of a four in-wheel motors electric vehicle.

As shown in Fig. 2, a driving condition of braking process with a specific initial velocity v_0, a terminal distance s_f and a terminal velocity v_f is considered in this study. The problem is how to optimize the regenerative energy while tracking the desired velocity. For this problem, we choose the uniform deceleration braking requirement v_2 to design the energy optimization controller. However, it is obvious that the braking velocity could also be an optimization variable to reduce the energy consumption. In this study, we aim to find the optimal velocity trajectory to improve the energy recovery of an electric vehicle.

B. CONTROL-ORIENTED MODELING

1) VEHICLE DYNAMICS MODEL

The half electric vehicle diagram with a slope is shown in Fig. 3. It includes the longitudinal motion and the rotational movement of the wheels. In addition, a single braking wheel diagram is given in Fig. 4. The dynamic formulations of the vehicle and the single wheel during the braking process is described as follows [18],

$$M\dot{v}_x = -F_{xf} - F_{xr} - F_s - F_a, \tag{1}$$

$$J_j\dot{\omega}_{wj} = \frac{1}{2}(R_eF_{xj} - T_{bj}), \quad j = f, r, \tag{2}$$

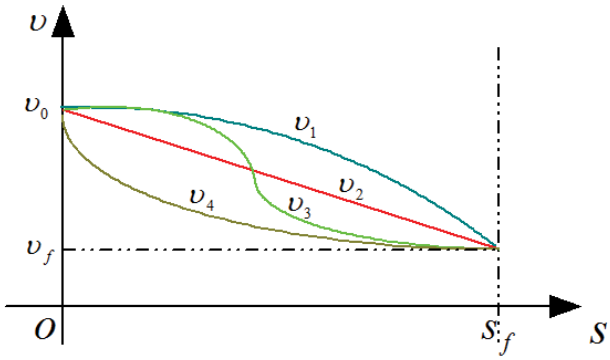

FIGURE 2. Optimization problem diagram.

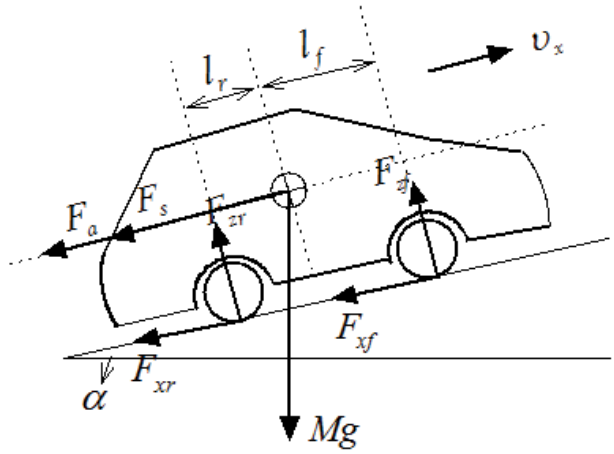

FIGURE 3. Half vehicle diagram.

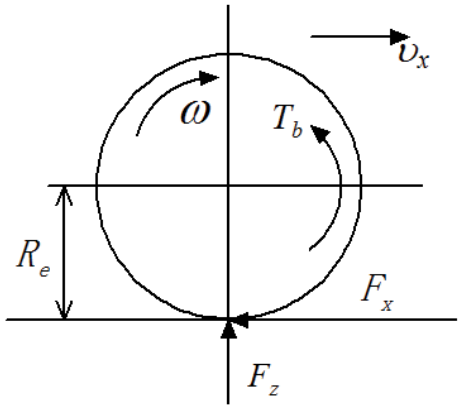

FIGURE 4. Single braking wheel diagram.

where v_x is the vehicle velocity. The rolling resistance is very small and is ignored in equation (1). F_{xf} and F_{xr} are the longitudinal braking forces between the road and the front and rear tires. J_j and ω_{wj} are respectively the rotational inertia and the rotary velocity of front and rear wheels, R_e is the effective rolling radius of the tires, T_{bj} is the braking torque of front and rear wheels.

The braking force F_{xf} and F_{xr} can be obtained by the normal load of the tires and the friction coefficient between the tires and the road. According to the Magic Formula model [22], the friction coefficient μ is a nonlinear function of the slip ratio κ which is given as follows,

$$F_{xj} = \mu_j(\kappa) F_{zj}. \tag{3}$$

$$\mu_j(\kappa) = D_x \sin\{C_x \arctan[B_x\kappa_j - E_x(B_x\kappa_j - \arctan(B_x\kappa_j))]\}, \tag{4}$$

$$\kappa_j = \frac{\omega_{wj} R_e - v_x}{v_x}. \tag{5}$$

where F_{zj} is the normal load of the front and rear tires, B_x, C_x, D_x, E_x are respectively the stiffness, shape, peak and curvature factor of the tires, which can be calculated with vehicle parameters. The longitudinal slip ratio describes the difference between the actual longitudinal velocity at the axle of the wheel and the equivalent rotational velocity of the tire. The normal load of the front and rear tires can be calculated as follows,

$$F_{zf} = \frac{1}{l_f + l_r}(Mgl_r \cos\alpha - Mgh \sin\alpha - Ma_x h), \tag{6}$$

$$F_{zr} = \frac{1}{l_f + l_r}(Mgl_f \cos\alpha + Mgh \sin\alpha + Ma_x h). \tag{7}$$

where l_f and l_r are respectively the longitudinal distance from center of gravity to front and rear tires, g is the acceleration due to gravity, h is the distance from center of gravity to ground of the vehicle.

2) IN-WHEEL MOTOR AND BATTERY MODEL

The in-wheel motor has been studied again widely because of its advantages of the flexible system layout, higher transmission efficiency and the direct independent control of each electric wheel, which make the vehicle dynamic control more flexible and easy to realize the regenerative braking control [14]–[16]. Only the regenerative mode of the in-wheel motor is considered in this study, the braking torque limitation is shown in Fig. 5. T_m and ω_m are respectively the braking torque and the rotary velocity of the in-wheel motor. The braking torque is limited by three boundaries; $T_{m,max}$ is the maximum torque at low rotary velocity caused by the current limitation. P_{max} is the maximum power limited by the current and voltage. $\omega_{m,max}$ is the maximum rotary velocity limited by the mechanical strength.

The in-wheel motor is simplified by a first-order model with a torque time constant τ, and is described as [15],

$$T_m = \frac{1}{\tau s + 1} T_{m,ref}, \tag{8}$$

where $T_{m,ref}$ is the reference braking torque. The final braking torque work on the wheel equals the actual braking torque of the in-wheel motor amplified with the reduction gear ratio, which is expressed as follows,

$$T_w = g_0 T_m, \tag{9}$$

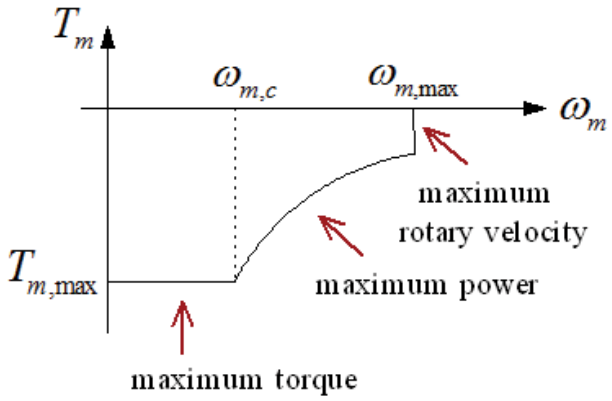

FIGURE 5. In-wheel motor torque limitation.

$$\omega_w = \frac{1}{g_0}\omega_m, \tag{10}$$

where T_w is the braking torque on the wheel, g_0 is the transmission ratio of the reduction gear, ω_w is the rotary velocity of the wheel.

An typical model of electrochemical battery suited to model the energetic behavior is used in this study. The equivalent electrical circuit consists a variable voltage source and a variable resistance, they are functions of the state of charge (SOC) and the temperature. The charging efficiency of the battery is also a function of the SOC and the electric current. The charging energy loss which is related with the battery characteristics is not considered in this optimization problem. The regenerative energy E_r is considered as the energy before the charge of the battery, it can be described as follows.

$$E_r = \int_0^{t_f} U_b I_b dt, \tag{11}$$

where U_b and I_b are respectively the front voltage and current of the battery, t_f is the final time of the regenerative braking process.

3) POWER FLOW MODEL

There are two braking modes in the regenerative braking system, the regenerative braking and friction braking. In order to recover the electric energy as much as possible, the series braking strategy [17] is used in this research. This strategy changes to the friction braking mode only if the total braking demand exceeds the limit of regenerative braking mode. During the regenerative braking process, the mechanical power is converted to electrical power and charged into the battery. The energy regeneration process can be described as

$$E_r = E_0 - E_{loss1} - E_{loss2} - E_{loss3}, \tag{12}$$

where E_0 is the initial kinetic of the electric vehicle. E_{loss1} is the energy loss caused by the rolling resistance, gradient resistance and aerodynamic drag resistance which are related to the vehicle speed and the slope of the road. E_{loss2} is the energy loss caused by the copper and iron loss and the mechanical loss inside of the motor. E_{loss3} is the energy loss caused by the hydraulic braking system, such as the mechanical friction loss and the pressure loss.

TABLE 1. Main parameters of in-wheel motors.

Parameter	Value
Torque time constant (τ)	0.1s
Maximum torque ($T_{mj,max}$)	118Nm
Maximum rotary velocity ($\omega_{mj,max}$)	9000rpm
Maximum power ($P_{mj,max}$)	26KW

The initial kinetic energy is defined as

$$E_0 = \frac{1}{2}Mv_0^2, \tag{13}$$

where M is the total mass of the vehicle. According to equation (12), it can be seen that in order to improve the regenerative efficiency of the electric vehicle during a braking process, the optimization problem is to minimize the total energy loss. E_{loss1} can be described as follows,

$$E_{loss1} = \int_0^{t_f} P_{loss1} dt, \tag{14}$$

$$P_{loss1} = (F_r + F_a + F_s)v_x, \tag{15}$$

where P_{loss1} is the energy loss power, F_r, F_a, F_s are respectively the rolling resistance, aerodynamic drag resistance, and gradient resistance. They can be calculated by the following formulations.

$$F_r = C_r Mg\cos\alpha, \tag{16}$$

$$F_a = \frac{1}{2}C_a A\rho v_x^2, \tag{17}$$

$$F_s = Mg\sin\alpha, \tag{18}$$

where C_r is the rolling resistance coefficient, α is the road slope which is considered as a constant in this research. C_a, A, and ρ are respectively the aerodynamic drag coefficient, the frontal area of the vehicle and the mass density of the air.

The second energy loss E_{loss2} can be described with the motor to battery efficiency η_m, which is defined as equation (19).

$$\eta_m = \frac{U_b I_b}{T_m \omega_m}, \tag{19}$$

where $T_m\omega_m$ and U_bI_b are respectively the input power P_{in} and output power P_{out} of the in-wheel motor. As U_bI_b is a function of T_m and ω_m, the motor to battery efficiency can be described as $\eta_m(t) = f(T_m(t), \omega_m(t))$, which can be obtained by the experimental data of the in-wheel motor. In this paper, the motor to battery efficiency is calculated by the motor energy loss map of AMESim software, which is also a function of the motor torque and rotary velocity. The in-wheel motor efficiency maps and the main parameters are respectively given in Fig. 6 and Table 1. The left and right sides of the vehicle is considered the same in this research.

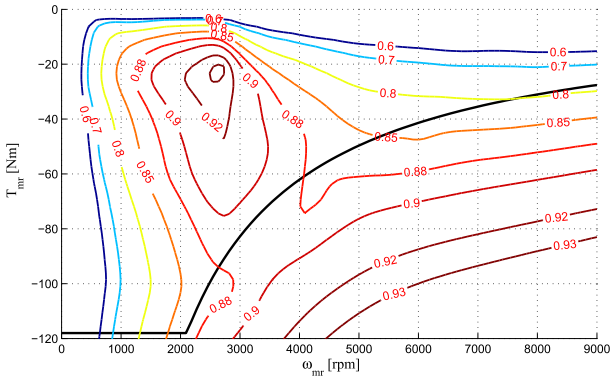

FIGURE 6. Efficiency of the in-wheel motor.

Based on the motor to battery efficiency, E_{loss2} can be expressed as,

$$E_{loss2} = \int_0^{t_f} P_{loss2} dt, \tag{20}$$

$$P_{loss2} = 2(1-\eta_{mf})T_{mf}\omega_{mf} + 2(1-\eta_{mr})T_{mr}\omega_{mr}. \tag{21}$$

where P_{loss2} is the total power loss corresponding to E_{loss2}, η_{mf} and η_{mr} are respectively the motor to battery efficiency of front and rear in-wheel motors. T_{mf}, T_{mr} and ω_{mf}, ω_{mr} are the torque and rotary velocity of front and rear in-wheel motors.

The hydraulic energy loss can be described as follows,

$$E_{loss3} = \int_0^{t_f} P_{loss3} dt, \tag{22}$$

$$P_{loss3} = T_{hf}\omega_{wf} + T_{hr}\omega_{wr}, \tag{23}$$

where T_{hf} and T_{hr} are the hydraulic braking torque of front and rear wheels.

III. BRAKING ENERGY OPTIMIZATION DESIGN

According to the above optimization problem statement and the dynamics formulations, the velocity optimization is equivalent to find the solution of control policy $u(t) = [T_{mf}, T_{mr}, T_{hf}, T_{hr}]^T, t \in [0, t_f]$, i.e. the motor and hydraulic braking torque on front and rear wheels.

A. MPC BASED VELOCITY-TRACKING CONTROLLER

For the driving condition with desired velocity, one of the control targets is that the total braking torque of hydraulic and in-wheel motor braking torque need to track the desired braking requirement. The desired braking torque is calculated by the braking control signal, which is provided by the driver model with a PID controller.

$$T_{ref} = z(-4g_0 T_{m,max}(\omega) - T_{h,max}), \tag{24}$$

$$z = -K_p V_e - K_i \int V_e dt - K_d \dot{V}_e, \tag{25}$$

$$V_e = V_r - V_x, \tag{26}$$

where z represents the braking control signal, its value is in the range of [0, 1] (0 = no braking; 1 = maximum braking). $T_{h,max}$ is the maximum hydraulic braking torque. V_e is the error between the reference speed and the actual vehicle speed. The braking torque error can be described as follows,

$$\begin{aligned} T_e &= T_{total} - T_{ref} \\ &= 2(g_0 T_{mf} + g_0 T_{mr} + T_{hf} + T_{hr}) - T_{ref}. \end{aligned} \tag{27}$$

Then the total energy optimization problem is formulated as,

$$\begin{aligned} &\min_{U(t)} \int_0^{t_f} F(x,u,t')dt', \\ &\quad F(x,u,t) = W_1 T_e^2(t) + W_2 P_{loss2}(t) \\ &\quad + W_3 P_{loss3}(t) \\ &\quad = W_1[T_{total}(t) - T_{ref}(t)]^2 \\ &\quad + W_2[2(1-\eta_{mf}(t))\omega_{mf}(t)T_{mf}(t) \\ &\quad + 2(1-\eta_{mf}(t))\omega_{mf}(t)T_{mf}(t)] \\ &\quad + W_3[T_{hf}(t)\omega_{wf}(t) + T_{hr}(t)\omega_{wr}(t)] \end{aligned} \tag{28}$$

$$s.t.\ \ \dot{v}_x(t) = \frac{1}{M}[-F_{xf}(t) - F_{xr}(t) - F_s(\alpha) - F_a(t)], \tag{29a}$$

$$\dot{s}(t) = v_x(t), \tag{29b}$$

$$\dot{\omega}_{wj}(t) = \frac{1}{2J_j}[R_e F_{xj}(t) - T_{bj}(t)], \tag{29c}$$

$$0 \le T_{mj}(t) \le T_{mj,max}(t), \tag{29d}$$

$$0 \le T_{hj}(t) \le T_{hj,max}, \tag{29e}$$

$$0 \le \omega_{mj}(t) \le \omega_{mj,max}, \tag{29f}$$

where W_1, W_2, W_3 are the weights of three cost functions, $x(t) = [v_x, s, \omega_{wj}]^T$ is the state vector. The equations of $\dot{v}_x$, $\dot{s}$, $\dot{\omega}_{wj}$ are the state equation constraints, the three inequalities are the saturation constraints of the actuators. The real-time maximum braking torque of the motor is a function of the rotary velocity, which is described as follows,

$$T_{mj,max}(t) = \begin{cases} T_{mj,max}, & \omega_{mj}(t) \le \dfrac{P_{mj,max}}{T_{mj,max}} \\ \dfrac{P_{mj,max}}{\omega_{mj}(t)}, & \omega_{mj}(t) > \dfrac{P_{mj,max}}{T_{mj,max}} \end{cases} \tag{30}$$

where $T_{mj,max}$ and $P_{mj,max}$ are respectively the maximum braking torque and power of the in-wheel motor.

In order to find the real-time solution of the formulated optimization problem, the model predictive control method is used to design the controller, which is one of the most effective methods to deal with a control problem with multiple constraints [19], [20]. The basic theory of MPC can be described as, at every sampling moment, according to the current measurement state information to obtain the solution of a finite time optimization problem. Then apply the first element of the control sequence to the controlled plant, repeat this process with the new measurement to the new optimization problem at the next sampling time [21].

According to the MPC theory, the optimization problem (28) is reformulated as a discrete form,

$$\min_{U_k} J(x(k), U_k) = \sum_{i=0}^{p} F[x(k+i|k), u(k+i|k)],$$
$$U_k \underline{def} \{u(k|k), u(k+1|k), ..., u(k+p|k)\} \quad (31)$$
$$s.t.\ \dot{v}_x(k) = \frac{1}{M}[-F_{xf}(k) - F_{xf}(k) - F_s(\alpha) - F_a(k)], \quad (32a)$$
$$\dot{s}(k) = v_x(k), \quad (32b)$$
$$\dot{\omega}_{wj}(k) = \frac{1}{2J_j}[R_e F_{xj}(k) - T_{bj}(k)], \quad (32c)$$
$$0 \le T_{mj}(k) \le T_{mj,max}(k), \quad (32d)$$
$$0 \le T_{hj}(k) \le T_{hj,max}, \quad (32e)$$
$$0 \le \omega_{mj}(k) \le \omega_{mj,max}, \quad (32f)$$

where k is the current time, p is the predictive horizon. U_k is the dependent control variable of the predictive system. $u(k+1|k)$ indicates the predicted control input of time $k+1$ at the current time k. Equations (32a),(32b) and (32c) are the discrete form of the state space model, which can be described as $\dot{x}(k) = f(x(k), u(k))$. According to the model predict theory, the future state of the system can be predicted based on the current measurement states. At the current instant k, the system predictive equation can be derived based on the forward Euler method,

$$\begin{aligned} x(k+1|k) &= x(k) + f(x(k), u(k))T_s, \\ x(k+2|k) &= x(k+1|k) + f(x(k+1|k), u(k+1))T_s, \\ &\vdots \\ x(k+p(k)|k) &= x(k+p(k)-1|k) + f(x(k+p(k)-1|k), \\ &\quad u(k+p(k)-1))T_s, \end{aligned} \quad (33)$$

where T_s is the system sampling time.

B. MPC BASED VELOCITY OPTIMIZATION CONTROLLER

For the velocity optimization problem, because the velocity has a certain influence on the energy loss P_{loss1}, so it should be considered in the cost function. In addition, the constraint of the terminal velocity and distance are involved in this strategy. The total energy optimization problem can be formulated as follows,

$$\min_{U(t)} \int_0^{t_f} (V_1 P_{loss1}(t') + V_2 P_{loss2}(t') + V_3 P_{loss3}(t'))dt',$$
$$\text{s.t. (29a) to (29f)}, \quad (34)$$
$$s(t_f) = s_f, \quad (35)$$
$$v(t_f) = v_f, \quad (36)$$

where V_1, V_2, V_3 are the weights of three energy loss power, the constraints of the state space equations and the actuator saturation constraints are the same as in velocity-tracking control. $s(t_f)$ and $v(t_f)$ are the terminal state constraints.

In order to obtain the desired terminal velocity, the constraint $v(t_f)$ is converted into a terminal state penalty term of the cost function. Therefore, the optimization problem (34) is changed into the problem (37) as follows, subjected to constraints (29a) to (29f) and constraint (35).

$$\min_{U(t)} J = \int_0^{t_f} G(x, u, t')dt' + \varphi(x(t_f)), \quad (37)$$

where

$$\begin{aligned} G(x, u, t) = V_1[&\frac{1}{2}C_a A \rho v_x^2(t) + Mg \sin\alpha v_x(t)] \\ &+ V_2[2(1-\eta_{mf}(t))\omega_{mf}(t)T_{mf}(t) \\ &+ 2(1-\eta_{mr}(t))\omega_{mr}(t)T_{mr}(t)] \\ &+ V_3[T_{hf}(t)\omega_{wf}(t) + T_{hr}(t)\omega_{wr}(t)], \end{aligned} \quad (38)$$
$$\varphi(x(t_f)) = V_4[v(t_f) - v_f]^2. \quad (39)$$

Because of the specific terminal velocity and distance constraints of this optimization problem, the terminal time t_f will be a potential optimal variable, not a fixed constant. Therefore, in order to solve the constraints of terminal velocity and distance, the optimization problem will be transformed from the time horizon to the distance horizon. In other words, the system sampling time will be changed into sampling distance. In addition, since the terminal velocity needs to be predicted at each sampling distance to satisfy the constraint, the predictive distance horizon recedes gradually for each renewed optimization problem. Therefore, the final transformed optimization problem can be described as equation (40), subject to constraints (32a) to (32f).

$$\min_{U_k} J(x(k), U_k) = \sum_{i=0}^{p} F[x(k+i|k), u(k+i|k)] + \varphi[x(k+p|k)], \quad (40)$$
$$p(k) = int(\frac{s_f - s(k)}{\Delta s(v_x)}), \quad (41)$$

where $p(k)$ is the receding predictive horizon related to the remaining distance. To be simple, the control horizon of the MPC method is set the same with the predictive horizon. $\Delta s(v_x)$ is the system sampling distance, it is designed as a function of the velocity to reduce the predict states error caused by the sampling distance step. At the current instant k, the system predictive equation can be derived based on the forward Euler method and the derivative equation $\dot{x}(s) = \dot{x}(t)/\dot{s}(t)$,

$$\begin{aligned} x(k+1|k) &= x(k) + \frac{f(x(k), u(k))}{v_x(k)}\Delta s, \\ x(k+2|k) &= x(k+1|k) + \frac{f(x(k+1|k), u(k+1))}{v_x(k+1|k)}\Delta s, \\ &\vdots \\ x(k+p(k)|k) &= x(k+p(k)-1|k) \\ &\quad + \frac{f(x(k+p(k)-1|k), u(k+p(k)-1))}{v_x(k+p-1|k)}\Delta s. \end{aligned} \quad (42)$$

C. ONLINE SOLUTION FOR THE OPTIMIZATION PROBLEM

Generally, due to the constraints of the system, it is not available to get the analytical solution directly for the optimization problem. The commonly used iterative solution methods are mainly active set method, interior point method etc. However, the calculation steps of these algorithms are cumbersome and time consuming. Since the Particle Swarm Optimization (PSO) algorithm has less constraints and the iteration process of it is simpler, it is used to improve the computational efficiency of the optimization problem. The basic theory of PSO is to find the optimal solution based on iteration method starting with a random solution. The particles are updated at each generation according to their self experience and group experience, and the quality of the particles are evaluated by the fitness function. Each particle could be the potential optimal solution of the optimization problem [23], [24]. The particles position in the search space are updated based on the following transition rule,

$$V_i^{t+1} = wV_i^t + c_1\, r_1(P_i^t - X_i^t) + c_2\, r_2(P_g^t - X_i^t), \quad (43a)$$

$$X_i^{t+1} = X_i^t + V_i^{t+1}, \quad (43b)$$

where t is the iteration number, $i = 1, 2, \cdots, N$, N is the size of the particle swarm. $X_i = (x_{i1}, x_{i1}, \cdots, x_{iD})$ and $V_i = (v_{i1}, v_{i1}, \cdots, v_{iD})$ are respectively the position and the position update velocity of particle i, D is the dimension of the search space. $P_i = (p_{i1}, p_{i2}, \cdots, p_{iD})$ and $P_g = (p_{g1}, p_{g2}, \cdots, p_{gD})$ respectively represent the optimal particle at the current time among its different generations and the entire particle swarm. particle i and and. w is the inertia weight of the particle i, c_1 and c_2 are respectively the cognitive and social factor, r_1 and r_2 are random numbers uniformly distributed within the range $[0, 1]$. These parameters are very important to satisfy the convergence and the computational performance of PSO solution. They are selected by the empirical values in this study.

For the optimization problem (37), the fitness function of the particles can be expressed as $f(x(k), X_i) = J(x(k), U_k)$, thus the optimal particle can be selected by the following regulation,

$$f(x(k), P_i) = min\{f(x(k), X_i^t), f(x(k), X_i^{t+1}), \cdots, f(x(k), X_i^T)\},\ i = 1, 2, \cdots, N \quad (44a)$$

$$f(x(k), P_g) = min\{f(x(k), P_i),\ i = 1, 2, \cdots, N\}, \quad (44b)$$

where T is the total iteration number, P_i is the optimal generation of the particle i, P_g is the optimal particle of the swarm and the optimal solution of the optimization problem, i.e. $U_k^*(k) = P_g$. The first element of $U_k^*(k)$, which is shown in equation (45), will be taken as the control input of the system. Then we use the latest measurements of the system states to refresh and resolve the renewed optimization problem at each sampling instant until the last step.

$$u^*(k) = [1, 0, ..., 0]U_k^*(k) \quad (45)$$

IV. SIMULATIONS AND ANALYSIS

A few simulation results and analysis are presented in this section to demonstrate the validity of the proposed braking energy management strategy. The four in-wheel motor electric vehicle model is built in AMESim software, which consists of the vehicle dynamics module, the suspension system module, the Magic Formula tire module, the in-wheel motors module and a high power dynamic battery pack module. The co-simulation is carried out based on AMESim and Simulink/MATLAB. The main parameters of the electric vehicle are listed in Table 2.

TABLE 2. Key parameters of electric vehicle.

Definition	Symbol	Value
Vehicle mass	M	1430 kg
Height of vehicle c.g.	h	0.37 m
Distance from c.g. to front axle	l_f	1.06 m
Distance from c.g. to rear axle	l_r	1.34 m
Effective radius of the tire	R_e	0.29 m
Reducer ratio	g_0	5
Aerodynamic drag coefficient	Ca	0.34
Air mass density	ρ	1.22 kg/m^3
Frontal area of the vehicle	A	2.08 m^2

The simulations are respectively conducted under three different conditions. The first one is with a low deceleration on a flat road, the hydraulic braking mode will not work in this simulation. The second one is the same road condition with a high deceleration in which the hydraulic braking mode will be involved to compensate for the deficiency due to the constraint of in-wheel motor, to attain the braking requirement. The third one is conducted on a flat-slope road with a high deceleration. Under each simulation condition, the proposed MPC velocity-tracking controller and velocity optimization controller are compared with a rule-based velocity-tracking controller. The hydraulic and motor braking distribution in the rule-based controller is based on the series braking method, and the front and rear wheel braking distribution is based on the normal load proportion on front and rear wheels.

In this paper, the regeneration efficiency is defined as the ratio between the regenerative energy E_r and the kinetic energy E_0 at the initial moment of braking, which can be expressed as follows,

$$\xi = \frac{E_r}{E_v}, \quad (46)$$

$$E_r = \int_0^{t_f} P_{out}\, dt, \quad (47)$$

A. SIMULATIONS ON FLAT ROAD

1) LOW DECELERATION

According to the formulated control problem, the braking requirement in this simulation condition is set as follows: the initial velocity is 25 m/s, the terminal distance and velocity are respectively 106 m and 10 m/s. For the MPC velocity optimization strategy, the sample distance is designed by $\triangle s = 0.1\ v_x$, so it changes from 2.5 m to 1 m.

The corresponding predictive horizon is from 42 to 0. For the rule-based and MPC velocity-tracking strategy, the corresponding desired uniform deceleration is 2.48 m/s^2. The predictive horizon for MPC velocity-tracking strategy is 5 and the sample time is 0.01 s.

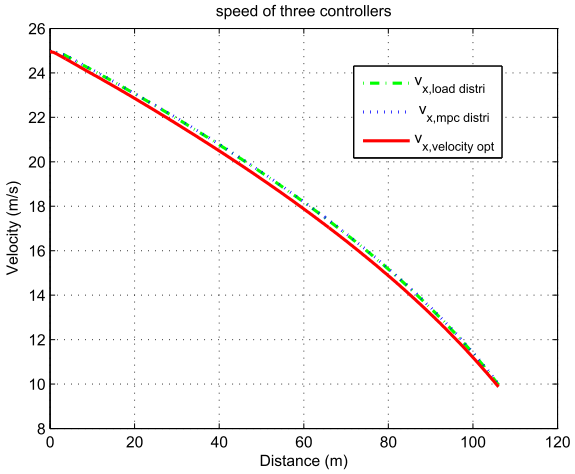

FIGURE 7. The velocity of three controllers.

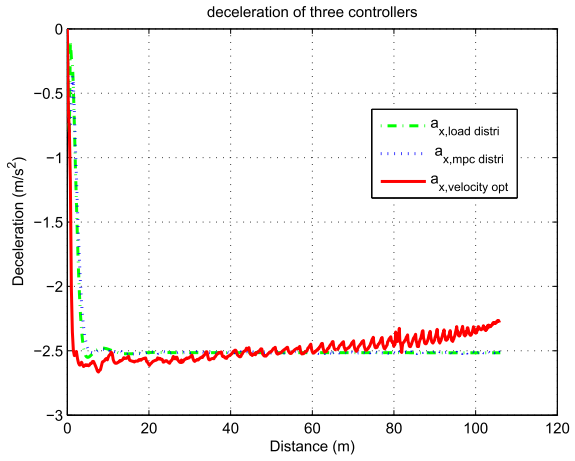

FIGURE 8. The deceleration of three controllers.

The actual velocity results of the three control strategies are shown in Fig. 7. It can be seen that the terminal velocities in these three methods at the destination are almost 10 m/s, which indicates that all of the strategies can achieve the braking requirement. It should be noted that because the desired deceleration is set in both rule-based and MPC velocity-tracking strategies. The braking time are the same for them, 6.04 s. However, since the velocity is an optimization variable in the velocity optimization strategy, the braking time is considered as an indirect optimization variable, the final optimal braking time is 6.13 s. It is not much different from the first two methods. Fig. 8 shows the deceleration of three methods. For the velocity optimization strategy, the deceleration at the preliminary stage is a little higher than other two strategies, but lower at the later stage.

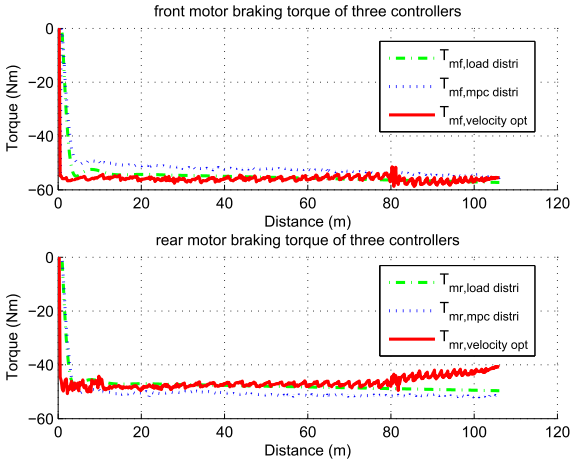

FIGURE 9. The motor braking torque of three controllers.

Under this simulation condition, the deceleration is low, so that the total braking requirement is within the range of the motor braking torque constraint. The motor braking torque distribution results on front and rear wheel of three controllers are given in Fig. 9. The front in-wheel motor braking torque of MPC method is higher than the rule-based method, but the rear in-wheel motor braking torque is lower. The distribution difference is because the front and rear motor-to-battery efficiencies are considered in MPC controller. The velocity optimization controller considered the influence of both the motor-to-battery efficiencies and the velocity to the energy recovery.

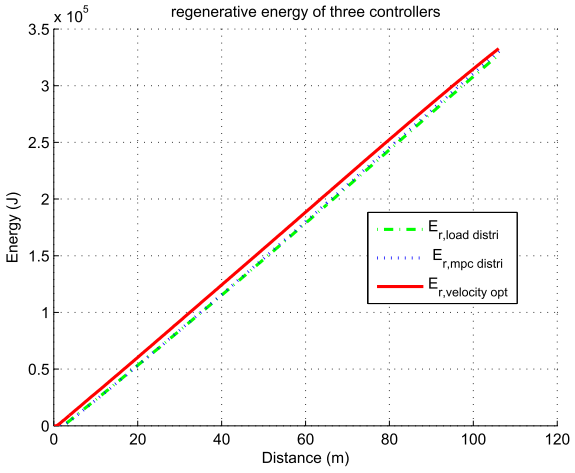

FIGURE 10. The regenerative energy of three controllers.

Fig. 10 shows the regenerative energy results of the three methods. The regenerative energy and the regeneration efficiency of rule-based strategy are 327.28 KJ and 73.24%. For the MPC velocity-tracking strategy, the regenerative energy and efficiency are 330.42 KJ and 73.94%, which is 0.96% improved than the rule-based strategy. For velocity optimization strategy, the regenerative energy and efficiency are 332.65 KJ and 74.44%, which is 1.64% improved than

TABLE 3. Comparison results of three strategies with low deceleration on a flat road.

Strategy	Rule-based	MPC	Vopt
Terminal distance (m)	106.05	106.14	106.04
Terminal velocity (m/s)	9.96	9.98	9.88
Terminal time (s)	6.04	6.04	6.13
Initial kinetic energy (KJ)	446.88	446.88	446.88
Regenerative energy (KJ)	327.28	330.42	332.65
Regeneration efficiency (%)	73.24	73.94	74.44
Efficiency improvement (%)	–	0.96	1.64

rule-based strategy. The comparison results of three methods in this simulation condition are listed in Table 3.

In order to evaluate the computational efficiency of different algorithms, the computational time of PSO, active-set and interior-point method are compared in this simulation case. For the fair comparison, all of these solution algorithm are carried out under the MPC velocity-tracking framework. The predictive horizon for MPC velocity-tracking strategy is 5 and the sample time is 0.01 s. It should be noted that the optimized effect of these algorithms are almost the same. The computational time comparison results are given in Table 4. It shows that the computational efficiency of the PSO algorithm is 15.64 and 21.09 times respectively faster than the active-set and interior-point algorithm.

TABLE 4. Comparison results of computational time of three algorithms under MPC velocity-tracking optimization.

Algorithm	PSO	Active-set	Interior-point
Average computational time (s)	0.11	1.72	2.32
Multiple of speed increase (%)	–	15.64	21.09

2) HIGH DECELERATION

In order to assess the controller effectiveness under a high deceleration driving condition, the desired braking distance is changed to 70 m, but the initial velocity and desired terminal velocity are still 25 m/s and 10 m/s. For the MPC velocity optimization strategy, the sample distance changes from 2.5 m to 1 m, the predictive horizon changes from 28 to 0. The predictive horizon and the sample time for MPC velocity-tracking strategy are 5 and 0.01 s.

For the rule-based and MPC velocity-tracking strategy, the corresponding desired uniform deceleration become to 3.78 m/s^2. Due to the high desired deceleration and the in-wheel motor braking torque constraint, the hydraulic braking mode will work to meet the total braking requirement.

The velocity and deceleration of the three strategies are respectively given in Figs. 11 and 12. It can be seen that all of the three controllers achieved the braking demand. All terminal velocities down to almost 10 m/s at the terminal distance. It should be discovered that the deceleration of the velocity optimization method is smaller at high speed and larger at low speed. As a result of this, the total braking torque could be smaller at the beginning, which makes the hydraulic braking intervention smaller. Because under the

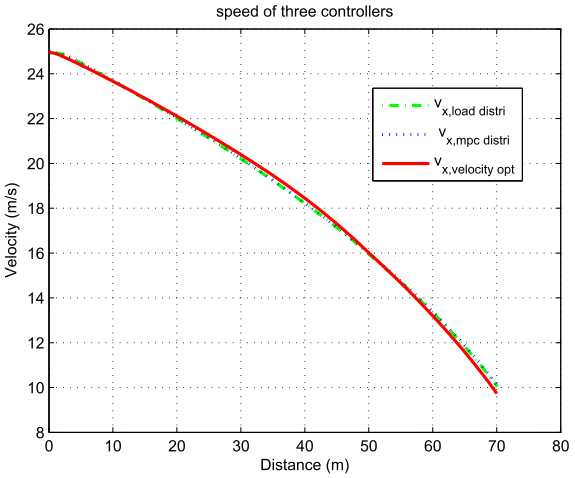

FIGURE 11. The velocity of three controllers.

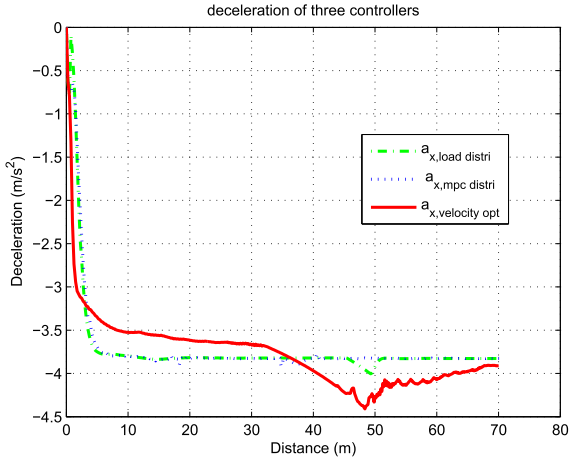

FIGURE 12. The deceleration of three controllers.

premise of the braking requirement can be obtained, the less the hydraulic braking is involved at the high speed stage, the more energy recovery by the motor braking is available at the low speed stage.

Figs. 13 and 14 show the distribution results of the motor braking torque and hydraulic braking torque. In the high speed part, the front wheel motor braking torque of the three controllers achieved the saturated braking torque. But because the normal force of the rear wheel is smaller, the motor braking torque of the rear wheel is smaller than other two strategies. It can be seen in Fig. 14, the hydraulic braking torque in velocity optimization method is the smallest and the working time is the shortest, which indicates the effectiveness of the control algorithm.

The regenerative energy of three strategies are given in Fig. 15. The regenerative energy and the regeneration efficiency of rule-based strategy are 291.05 KJ and 65.13%. For MPC velocity-tracking strategy, the regenerative energy and efficiency are 305.87 KJ and 68.45%, which is 5.1% improved than rule-based strategy. For velocity optimization

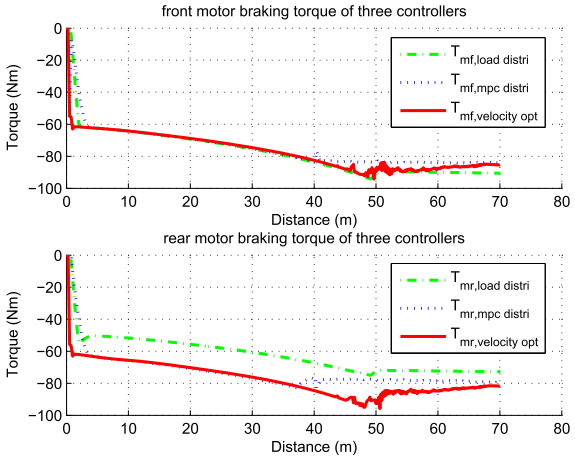

FIGURE 13. The motor braking torque of three controllers.

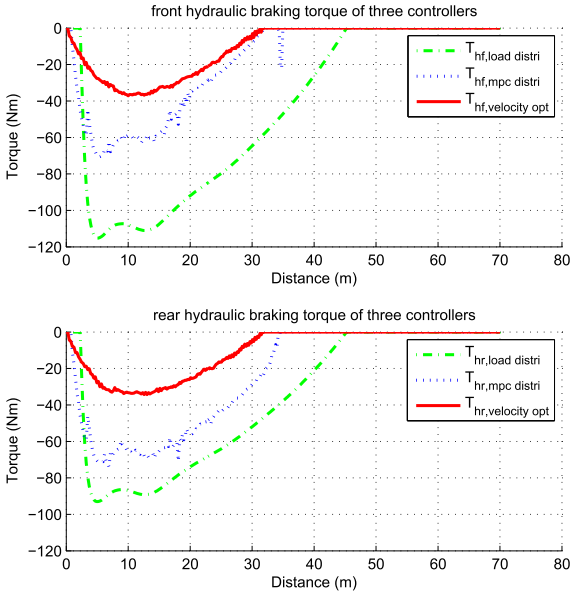

FIGURE 14. The hydraulic braking torque of three controllers.

strategy, the regenerative energy and efficiency are 318.05 KJ and 71.17%, which is 9.27% improved than rule-based strategy. The braking time are the same for the three controllers. The comparison results of the three methods under this simulation condition are listed in Table 5.

TABLE 5. Comparison results of three strategies with high deceleration on a flat road.

Strategy	Rule-based	MPC	Vopt
Terminal distance (m)	70.1	70.17	70.02
Terminal velocity (m/s)	10.04	10.07	9.73
Terminal time (s)	3.97	3.97	3.97
Initial kinetic energy (KJ)	446.88	446.88	446.88
Regenerative energy (KJ)	291.05	305.87	318.05
Regeneration efficiency (%)	65.13	68.45	71.17
Efficiency improvement (%)	–	5.1	9.27

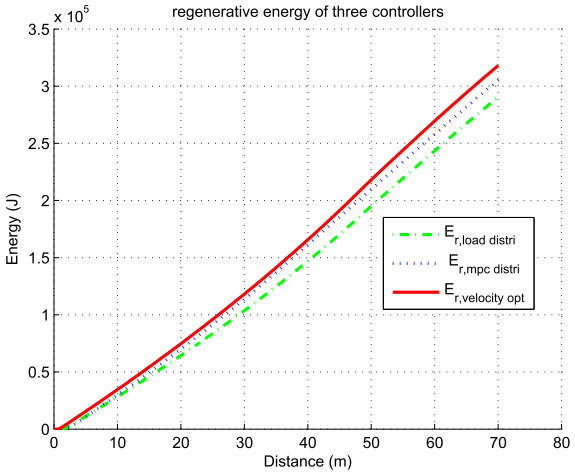

FIGURE 15. The regenerative energy of three controllers.

B. SIMULATIONS ON FLAT-SLOPE ROAD

In this section, the proposed controllers are evaluated on a flat-slope road with a high deceleration. The flat part is 45 m, the downhill slope is $-2°$ and the distance is 25 m. The initial velocity and desired terminal velocity are also set as 25 m/s and 10 m/s. For the MPC velocity optimization strategy, the sample distance changes from 2.5 m to 1 m, the predictive horizon changes from 28 to 0. The predictive horizon and the sample time for MPC velocity-tracking strategy are 3 and 0.01 s.The desired deceleration of rule-based and MPC velocity-tracking methods are still 3.78 m/s^2.

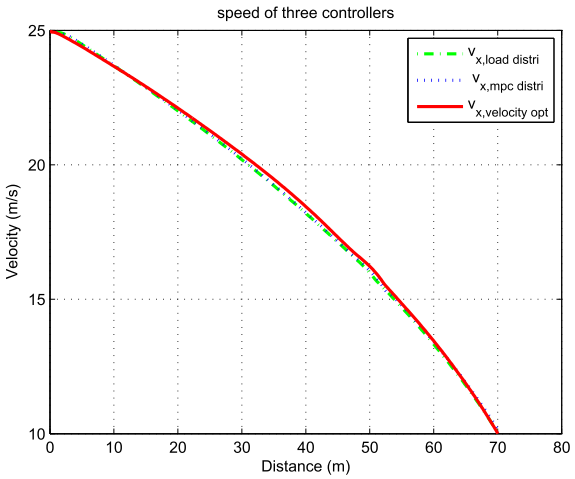

FIGURE 16. The velocity of three controllers.

The velocity and deceleration of three strategies are respectively given in Figs. 16 and 17. It can be seen that all of the three controllers achieved the braking demand. All terminal velocities are down to almost 10 m/s at the terminal distance. The vibration of deceleration at 45 m is because of the slope. The deceleration of velocity optimization method has the similar trend with the last simulation condition.

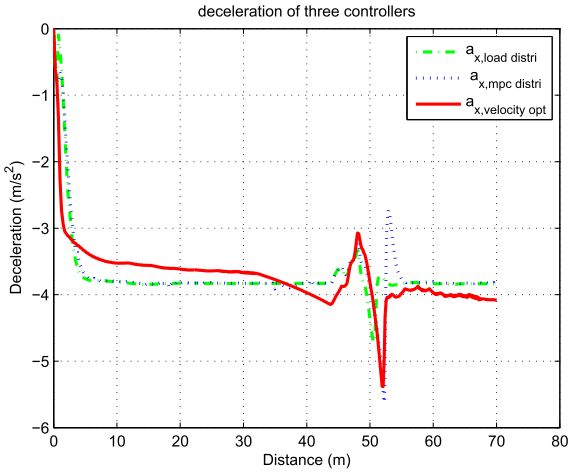

FIGURE 17. The deceleration of three controllers.

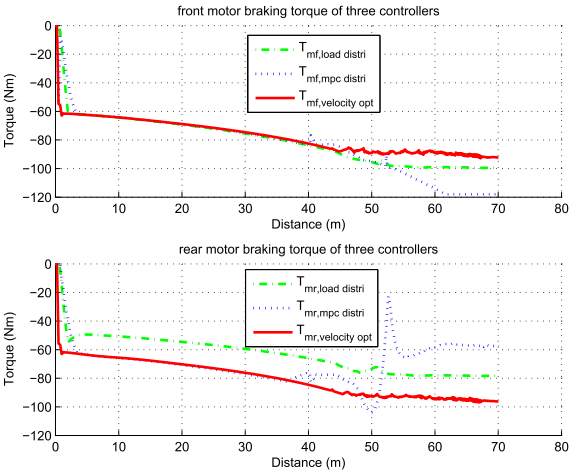

FIGURE 18. The motor braking torque of three controllers.

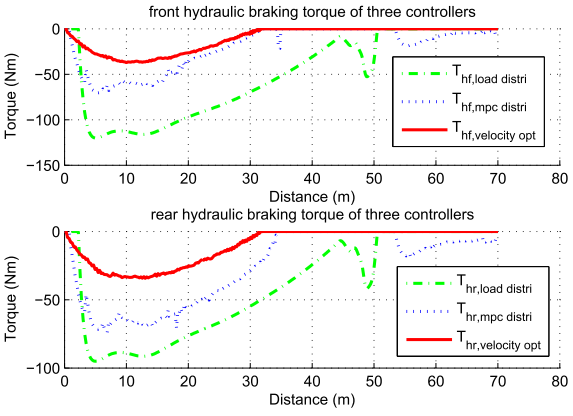

FIGURE 19. The hydraulic braking torque of three controllers.

Figs. 18 and 19 show the distribution results of motor braking torque and hydraulic braking torque. It can be seen that the total hydraulic braking torque of the velocity optimization method is less than the others, which makes greater possibilities for the energy recovery.

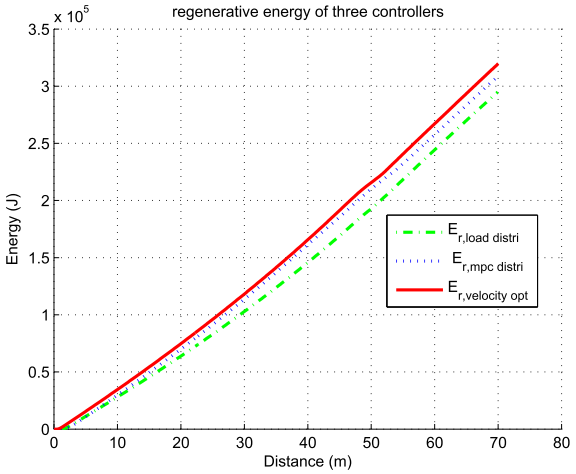

FIGURE 20. The regenerative energy of three controllers.

TABLE 6. Comparison results of three strategies with high deceleration on a flat-slope road.

Strategy	Rule-based	MPC	Vopt
Terminal distance (m)	69.95	70.09	70.03
Terminal velocity (m/s)	10.06	10.14	10
Terminal time (s)	3.96	3.96	3.94
Initial kinetic energy (KJ)	446.88	446.88	446.88
Regenerative energy (KJ)	294.86	309.35	319.76
Regeneration efficiency (%)	65.98	69.22	71.55
Efficiency improvement (%)	–	4.91	8.44

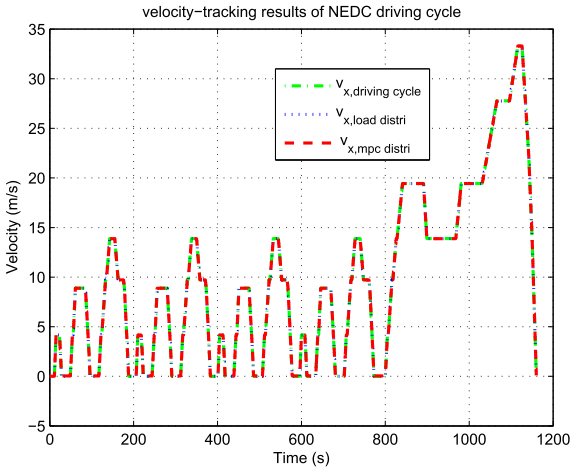

FIGURE 21. The velocity of NEDC.

The regenerative energy of the three strategies are given in Fig. 20. The regenerative energy and the regeneration efficiency of rule-based strategy are 294.86 KJ and 65.98%. For the MPC velocity-tracking strategy, the regenerative energy and efficiency are 309.35 KJ and 69.22%, which is 4.91% improved than rule-based strategy. For the velocity optimization strategy, the regenerative energy and efficiency are 319.76 KJ and 71.55%, which is 8.44% improved than rule-based strategy. The comparison results of the three methods in this simulation condition are listed in Table 6.

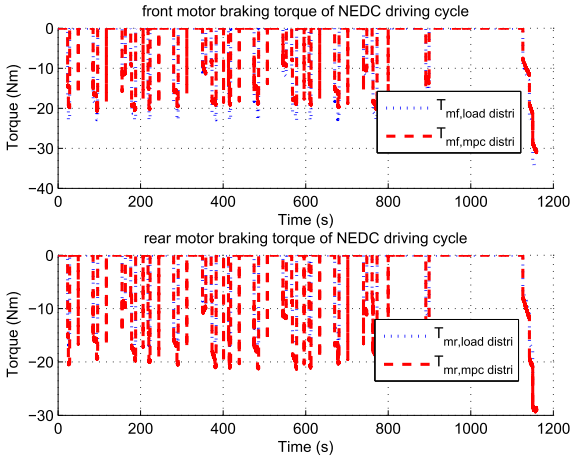

FIGURE 22. The motor braking torque of NEDC.

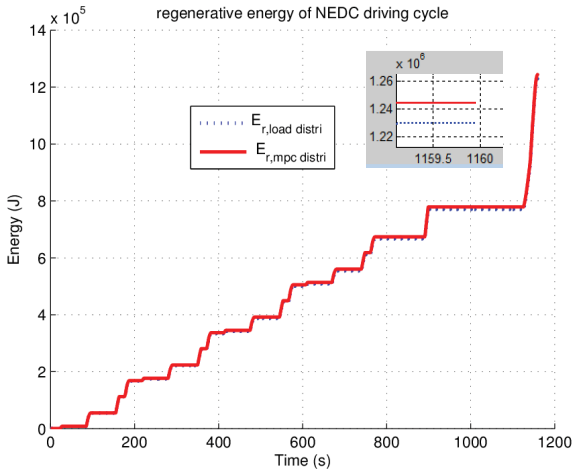

FIGURE 23. The regenerative energy of NEDC.

According to the above simulation results, the proposed velocity optimization controller has more advantage than the rule-based and MPC velocity-tracking controller, especially under the high deceleration driving condition and when the hydraulic braking is involved. However, the high speed and deceleration driving condition is not good for the energy recovery. In addition, the road grade can promote the regenerative efficiency.

C. SIMULATIONS UNDER NEDC DRIVING CYCLE

In this section, the rule-based and MPC velocity-tracking controller are evaluated under the New European Driving Cycle (NEDC). The predictive horizon for MPC velocity-tracking strategy is 5 and the sample time is 0.01 s.

Fig. 21 shows the velocity of NEDC and the velocity-tracking results of the rule-based and MPC controllers. It can be seen that they can track the velocity of the driving cycle very well. Fig. 22 shows the braking torque of the motors of the two strategies. Because the deceleration of the driving cycle is low, the hydraulic brake mode is not involved in this simulation condition. Fig. 23 and Table 7 shows the comparison results of the regenerative energy. It can be seen that, during the braking process of the driving cycle, the total regenerative energy of MPC velocity-tracking strategy is 1.17% improved than rule-based strategy.

TABLE 7. Comparison results of regenerative energy under NEDC.

Strategy	Rule-based	MPC
Regenerative energy (KJ)	1229.56	1243.95
Efficiency improvement (%)	–	1.17

V. CONCLUSION

In this paper, two regenerative braking energy management strategies are presented for an electric vehicle with four in-wheel motors. They are respectively designed based on MPC velocity-tracking and MPC velocity optimization methods. In both of the controllers, the main control idea is to distribute the hydraulic braking torque and the in-wheel motor braking torque between front and rear wheels. The optimal velocity trajectory is also attained through the braking torque distribution in the MPC velocity optimization method. In order to achieve the specific terminal velocity and distance constraints of the velocity optimization problem, a receding-horizon MPC controller is developed, and the conversion from the time horizon to the distance horizon is designed to satisfy the terminal constraints. In addition, the front and rear in-wheel motor to battery efficiency is considered to improve the regenerative efficiency of the braking process. To verify the effectiveness of the proposed MPC velocity tracking and MPC velocity optimization methods, three sets of simulations based on AMESim and Simulink co-simulation platform are conducted. Different driving conditions with low and high decelerations on flat and sloped roads are carried out. The simulation results are compared with a normal load distribution method, which demonstrate that the velocity optimization of the braking process can achieve the braking requirement and improve the energy efficiency of an electric vehicle. It should be noted that only a simple battery model is used in this research. The battery aging and charging efficiency will be considered in the future work based on this research.

REFERENCES

[1] W. Sierzchula, S. Bakker, K. Maat, and B. van Wee, "The competitive environment of electric vehicles: An analysis of prototype and production models," *Environ. Innov. Soc. Trans.*, vol. 2 pp. 49–65, Mar. 2012.

[2] L. Guo, H. Chen, B. Gao, and Q. Liu, "Energy management of HEVs based on velocity profile optimization," *Sci. China Inf. Sci.*, vol. 8, no. 62, pp. 1–3, 2018.

[3] Z. Junzhi, L. Yutong, L. Chen, and Y. Ye, "New regenerative braking control strategy for rear-driven electrified minivans," *Energy Convers. Manage.*, vol. 82, pp. 135–145, Jun. 2014.

[4] K. Itini, A. De Bernardinis, Z. Khatir, and A. Jammal, "Comparative analysis of two hybrid energy storage systems used in a two front wheel driven electric vehicle during extreme start-up and regenerative braking operations," *Energy Convers. Manage.*, vol. 144, pp. 69–87, Jul. 017.

[5] J. Chen, J. Yu, K. Zhang, and Y. Ma, "Control of regenerative braking systems for four-wheel-independently-actuated electric vehicles," *Mechatronics*, vol. 50, pp. 394–401, Apr. 2018.
[6] J. W. Ko, S. Y. Ko, I. S. Kim, D. Y. Hyun, and H. S. Kim, "Co-operative control for regenerative braking and friction braking to increase energy recovery without wheel lock," *Int. J. Automot. Technol.*, vol. 15, no. 2, pp. 253–262, 2014.
[7] J. Zhang, C. Lv, J. Gou, and D. Kong, "Cooperative control of regenerative braking and hydraulic braking of an electrified passenger car," *Proc. Inst. Mech. Eng., D, J. Automobile Eng.*, vol. 226, no. 10, pp. 1289–1302, 2012.
[8] C. T. Krasopoulos, M. E. Beniakar, and A. G. Kladas, "Velocity and torque limit profile optimization of electric vehicle including limited overload," *IEEE Trans. Ind. Appl.*, vol. 53, no. 4, pp. 3907–3916, Jul./Aug. 2017.
[9] M. A. S. Kamal, M. Mukai, J. Murata, and T. Kawabe, "Ecological vehicle control on roads with up-down slopes," *IEEE Trans. Intell. Transp. Syst.*, vol. 12, no. 3, pp. 783–794, Sep. 2011.
[10] C. Zhang, A. Vahidi, P. Pisu, X. Li, and K. Tennant, "Role of terrain preview in energy management of hybrid electric vehicles," *IEEE Trans. Veh. Technol.*, vol. 59, no. 3, pp. 1139–1147, Mar. 2010.
[11] G. Wu, K. Boriboonsomsin, and M. J. Barth, "Development and evaluation of an intelligent energy-management strategy for plug-in hybrid electric vehicles," *IEEE Trans. Intell. Transp. Syst.*, vol. 15, no. 3, pp. 1091–1100, Jun. 2014.
[12] Y. Chen, X. Li, C. Wiet, and J. Wang, "Energy management and driving strategy for in-wheel motor electric ground vehicles with Terrain profile preview," *IEEE Trans. Ind. Informat.*, vol. 10, no. 3, pp. 1938–1947, Aug. 2014.
[13] L. Guo, B. Gao, Y. Gao, and H. Chen, "Optimal energy management for HEVs in Eco-driving applications using bi-level MPC," *IEEE Trans. Intell. Transp. Syst.*, vol. 18, no. 8, pp. 2153–2162, Aug. 2017.
[14] F.-K. Wu, T.-J. Yeh, and C.-F. Huang, "Motor control and torque coordination of an electric vehicle actuated by two in-wheel motors," *Mechatronics*, vol. 23, pp. 46–60, Feb. 2013.
[15] B. Ren, H. Chen, H. Zhao, and L. Yuan, "MPC-based yaw stability control in in-wheel-motored EV via active front steering and motor torque distribution," *Mechatronics*, vol. 38, pp. 103–114, Sep. 2016.
[16] J. Hu, Y. Wang, Y. Gao, H. Fujimoto, and Y. Hori, "Robust yaw stability control for in-wheel motor electric vehicles," *IEEE/ASME Trans. Mechatronics*, vol. 22, no. 3, pp. 1360–1370, Jun. 2017.
[17] Y. Tanaka *et al.*, "Brake control device, and brake control method," U.S. Patent 8 733 849 B2, Dec. 24, 2009.
[18] R. de Castro, R. E. Araújo, and D. Freitas, "Wheel slip control of EVs based on sliding mode technique with conditional integrators," *IEEE Trans. Ind. Electron.*, vol. 60, no. 8, pp. 3256–3271, Aug. 2013.
[19] L. Guo, B. Gao, Y. Li, and H. Chen, "A fast algorithm for nonlinear model predictive control applied to HEV energy management systems," *Sci. China Inf. Sci.*, vol. 60, no. 9, 2017, Art. no. 092201.
[20] H. Guo, F. Liu, R. Yu, Z. Sun, and H. Chen, "Regional path moving horizon tracking controller design for autonomous ground vehicles," *Sci. China Inf. Sci.*, vol. 60, no. 1, 2017, Art. no. 013201.
[21] H. Chen, *Systems and Control Series: Model Predictive Control*, 1st ed. Beijing, China: Science Press, 2013.
[22] H. B. Pacejka, *Tyre and Vehicle Dynamics*, 2nd ed. London, U.K.: Elsevier, 2005.
[23] F. Xu, H. Chen, X. Gong, and Q. Mei, "Fast nonlinear model predictive control on FPGA using particle swarm optimization," *IEEE Trans. Ind. Electron.*, vol. 63, no. 1, pp. 310–321, Jan. 2016.
[24] F. Rajabi, B. Rezaie, and Z. Rahmani, "A novel nonlinear model predictive control design based on a hybrid particle swarm optimization-sequential quadratic programming algorithm: Application to an evaporator system," *Trans. Inst. Meas. Control*, vol. 38, no. 1, pp. 23–32, 2016.

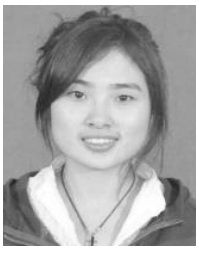

WEI XU received the B.S. degree in automation from the Harbin University of Science and Technology, Harbin, China, in 2010, and the M.S. degree in pattern recognition and intelligent system from Jilin University, Changchun, China, in 2015, where she is currently pursuing the Ph.D. degree in control theory and engineering. Her current research focuses on regenerative braking systems of electric vehicles.

HONG CHEN received the B.S. and M.S. degrees in process control from Zhejiang University, Zhejiang, China, in 1983 and 1986, respectively, and the Ph.D. degree in system dynamics and control engineering from the University of Stuttgart, Stuttgart, Germany, in 1997. Since 1999, she has been a Professor with Jilin University, Changchun, China, where she currently serves as a Tang Aoqing Professor and as the Director of the State Key Laboratory of Automotive Simulation and Control. Her current research interests include model predictive control, optimal and robust control, and nonlinear control and applications in mechatronic systems focusing on automotive systems.

JUNMIN WANG (SM'14) received the B.E. degree in automotive engineering and the M.S. degree in power machinery and engineering from Tsinghua University, Beijing, China, in 1997 and 2000, respectively, the M.S. degrees in electrical engineering and mechanical engineering from University of Minnesota Twin Cities, Minneapolis, MN, USA, in 2003, and the Ph.D. degree in mechanical engineering from The University of Texas at Austin, Austin, TX, USA, in 2007.

He also gained five years of full-time industrial research experience at the Southwest Research Institute (San Antonio Texas), from 2003 to 2008. He is currently the Accenture Endowed Professor in mechanical engineering with The University of Texas at Austin. In 2008, he started his academic career at The Ohio State University, where he founded the Vehicle Systems and Control Laboratory, was early promoted to Associate Professor, in 2013, and then very early promoted to Full Professor, in 2016. He has authored or coauthored more than 300 peer-reviewed publications, including 146 journal articles, and holds 13 U.S. patents. He has a wide range of research interests covering control, modeling, estimation, optimization, and diagnosis of dynamical systems, especially for automotive, smart, and sustainable mobility, human–machine, and cyber-physical system applications. He is an IEEE Vehicular Technology Society Distinguished Lecturer, an SAE Fellow, and an ASME Fellow. He was a recipient of numerous international and national honors and awards.

HAIYAN ZHAO received the B.S. degree in automation and the M.S. and Ph.D. degrees in control theory and control engineering from Jilin University, Changchun, China, in 1998, 2004, and 2007, respectively, where she has been a Lecturer, since 2007. Her current research interests include vehicle stability control and the state estimation of electric vehicles.